The structures and dipole moments of Ar–PF_3 and Kr–PF_3

Amine Taleb-Bendiab, Marabeth S. LaBarge, Lawrence L. Lohr, Robert C. Taylor, Kurt W. Hillig II, and Robert L. Kuczkowski
Department of Chemistry, University of Michigan, Ann Arbor, Michigan 48109

Robert K. Bohn
Department of Chemistry, University of Connecticut, Storrs, Connecticut 06268

(Received 22 December 1988; accepted 7 March 1989)

The complexes of PF_3 with Ar and Kr, were studied by Fourier transform microwave spectroscopy. The force constants and amplitudes of vibration for the van der Waals modes of the complexes and the average moments of inertia and structural parameters were estimated from the centrifugal distortion constants. The distance $(R_{c.m.})_{ave}$ between the rare-gas atom and the center of mass of PF_3 is 3.959 Å for the Ar complex and 4.077 Å for Kr while the angle $(\theta_{c.m.})_{ave}$ between the $R_{c.m.}$ vector and the C_3 axis of the PF_3 is 69.30° and 67.25°, respectively. The dipole moments of both complexes and of free PF_3 were determined. The induced dipole components estimated for the rare gas using electric fields from *ab initio* calculations of PF_3 agree with the experimental values for a conformation with the rare gas over a PF_2 face. The PF_2 face conformation is also consistent with the observed and *ab initio* estimates of the ^{83}Kr nuclear quadrupole coupling constant for the ^{83}Kr–PF_3 species.

I. INTRODUCTION

The microwave spectra of the weak complexes Ar–PF_3 and Kr–PF_3 were observed recently.[1,2] The spectra indicated that the complexes were asymmetric tops. The effective values for $R_{c.m.}$ (which joins the centers of mass of the two species) and the angle $\theta_{c.m.}$ (formed between $R_{c.m.}$ and the C_3 axis of PF_3) were 3.953 Å and 70.3° for Ar–PF_3 and 4.072 Å and 68.3° for Kr–PF_3. The internal orientation of the PF_3 could not be obtained from the moments of inertia, but symmetry considerations of the internal rotation potential function, noting the absence of free internal rotation or tunneling splittings in the spectrum, reduced the possibilities to the four positions for the rare-gas atom shown in Fig. 1. It was noted that the close approach of the fluorines to the rare gas atom in structures B and D made those conformations unlikely.

The number of assigned transitions for Ar–PF_3 has been considerably extended since the preliminary communication. They are reported here along with a force field analysis of the centrifugal distortion constants for both Ar–PF_3 and Kr–PF_3. This allows the average moments of inertia and structural parameters to be calculated. The dipole moments of both complexes and the ^{83}Kr nuclear electric quadrupole coupling constants have also been determined. This new information provides compelling evidence that structure C in Fig. 1 is the preferred conformation.

II. EXPERIMENTAL

Spectrometer

The rotational spectra were observed with a Fourier transform cavity microwave spectrometer employing a pulsed nozzle gas source.[1,2] The spectrometer has been recently modified to measure Stark effects.[3] The Stark splittings of the $J = 1 \leftarrow 0$ transitions of PF_3 and OCS (the calibrant[4]) and various transitions of the complexes were measured sequentially for a given electric field using an OCS/PF_3/Ar/Kr mixture (1:1:98:0 or 1:1:49:49). Ratios of shifts relative to OCS were analyzed in order to minimize calibration errors from power supply drift. Line widths were about 15 kHz (FWHM) at the highest fields (shifts of 2–3 MHz) and line centers were determined reproducibly to 1–3 kHz. The line width indicates a field homogeneity of better than 0.5% in the active volume of the cavity although the calibration gave fields some 12% smaller than calculated from the plate geometry. The origin of this discrepancy is unclear.

Centrifugal distortion constants

Forty-nine *a*- and *c*-dipole transitions involving J's between 0 and 11 were measured for Ar–PF_3. They were fit using the Watson *S*-reduction Hamiltonian (representation I^r) to five P^4 and two P^6 distortion constants[5,6] which are listed in Table I. The rms deviation $[\nu_{(obs)} - \nu_{(calc)}]$ of the fit was 2.0 kHz. The assigned transitions are available as

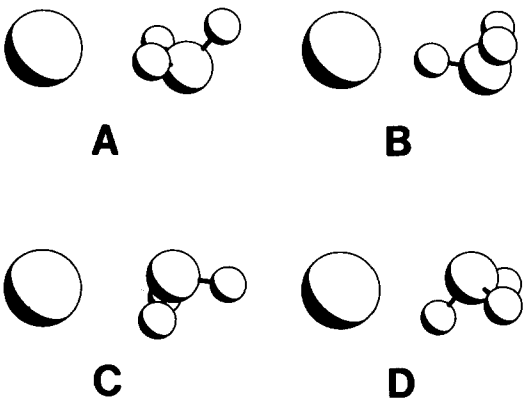

FIG. 1. Conformations of Ar–PF_3 and Kr–PF_3 which are consistent with the rotational constants.

 0021-9606/89/126949-07$02.10

supplementary material.[37] The constants[2] for the ^{84}Kr and ^{86}Kr isotopes of Kr–PF_2 are also listed in Table I for completeness along with the derived tau constants[5] employed in the force field analysis.

Quadrupole coupling constants

The ^{83}Kr isotope has a spin of 9/2 and a natural abundance of 11.5%. Using predictions for the unsplit positions based on the previous work,[2] 33 components from 7 transitions were assigned for the ^{83}Kr–PF_3 species. The quadrupole coupling constants and center frequencies were determined by least-squares fitting procedures using an algorithm which treats the quadrupole interactions as perturbations on the rotational energy.[7] The rotational and quadrupole coupling constants derived from the analysis are given in Table I. The rms deviation $[\nu_{(obs)} - \nu_{(calc)}]$ of the quadrupole fit was 3.2 kHz. The measured frequencies are available as supplementary material.[37]

Dipole moments

For the $J = 1 \leftarrow 0$ transitions of both OCS and PF_3, the Stark shift is given by $\Delta\nu = 8(\mu\mathscr{E})^2/15\nu_0 h^2$. Thus a plot of $\Delta\nu$(OCS) vs $\Delta\nu(PF_3)$ as $\mathscr{E}^2$ is varied should give a straight line with a slope independent of the field. A least-squares fit to the observed frequencies for fields from 130 to 600 V/cm yielded $\mu(PF_3) = 1.029(1)$ D [2σ unc.; previous value[8] is 1.03(1)D].

The Stark shifts for twelve M components from five transitions of Ar–PF_3 were measured at fields between 15 and 650 V/cm. Plots of $\Delta\nu/\mathscr{E}^2$ showed no significant curvature arising from nonsecond order effects. The dipole components of Ar–PF_3 were determined by a least-squares fit of the derived Stark coefficients (see Table II). Inclusion of a μ_b component in the fit gave $\mu_b^2 = -0.000\,41$, consistent with the expected value of 0. A similar procedure was followed for five M components of ^{84}Kr–PF_3 (Table II) except that fewer data were obtained resulting in a less precise determination.

III. ANALYSIS AND DISCUSSION

Force field and average structure

The values previously reported for the angle $\theta_{c.m.}$ between the $R_{c.m.}$ vector and the C_3 axis of the PF_3 were 70.3° and 68.3° for the Ar and Kr complexes, respectively. These were calculated from the so-called effective moments of inertia and ignore the vibrational contributions to the moments. It was of interest to evaluate the effect that the large amplitude motions associated with the van der Waals modes might have on these angles as well as on $R_{c.m.}$. Information about the intramolecular force field can be deduced from the centrifugal distortion constants leading to estimates of the force constants, amplitudes of vibration and the moments of inertia of the average configuration.[9]

The force field determination followed the procedure described for several other systems.[10] The harmonic force constants for Ar–PF_3, ^{84}Kr–PF_3 and ^{86}Kr–PF_3 were obtained from the τ's (Table I) by means of the Kivelson and Wilson relation[5]

$$\tau_{\alpha\beta\gamma\delta} = -\frac{\hbar^3}{4\pi}\cdot\frac{1}{I_{\alpha\alpha}I_{\beta\beta}I_{\gamma\gamma}I_{\delta\delta}}\sum_i\sum_j \mathbf{J}^i_{\alpha\beta} f_{ij}^{-1} J^j_{\gamma\delta}, \quad (1)$$

where α, β, etc. correspond to the a, b, or c inertial axes, f_{ij}^{-1} is the inverse force constant matrix element corresponding to the i and j internal coordinates and $J^i_{\alpha\beta}$ represent deriva-

TABLE I. Rotational and centrifugal distortion constants for Ar–PF_3 and Kr–PF_3. Quadrupole coupling constants for ^{83}Kr–PF_3.

	Ar–PF_3	^{84}Kr–PF_3[a]	^{86}Kr–PF_3[a]	^{83}Kr–PF_3[b]
A[c] (MHz)	7332.6087(7)[d]	7215.6640(13)	7215.3575(18)	7215.823(1)
B	1023.0563(1)	650.6089(2)	643.5480(2)	654.291(3)
C	952.5649(1)	622.1812(2)	615.7218(3)	625.452(7)
D_J (kHz)	3.5399(1)	1.3609(1)	1.3376(2)	1.05(4)
D_{JK}	60.19(3)	25.37(3)	25.11(8)	45.5(19)
D_K	143.78(8)	162.3(4)	162.3(6)	ND
d_1	−0.2453(4)	−0.0613(4)	−0.0599(8)	−0.31(3)
d_2	−0.0399(1)	−0.0064(3)	−0.0061(5)	ND
H_{JK}	−0.0032(3)	−0.0012(2)	ND[f]	ND
H_{KJ}	−0.023(1)	−0.015(1)	ND	ND
τ'_{aaaa}[e] (kHz)	−830.0(4)	−756.2(15)	−755.0(20)	
τ'_{bbbb}	−16.441(6)	−5.99(1)	−5.88(1)	
τ'_{cccc}	−12.516(6)	−5.00(1)	−4.92(1)	
τ'_1	−282.3(1)	−117.7(1)	−116.4(1)	
τ'_2 (MHz)	−38.94(1)	−109.7(1)	−107.5(1)	

[a]Reference 2.
[b]^{83}Kr quadrupole coupling constants (MHz): $\chi_{aa} = 4.31$ (1), $\chi_{bb} = -2.41$ (1), $\chi_{cc} = -1.90$ (1).
[c]Fitted spectral parameters. Watson S-reduction (I^r) (Ref. 5).
[d]Uncertainty in parentheses (1σ).
[e]τ's, determinable parameters using relationships in Ref. 4.
[f]ND = not determined.

TABLE II. Stark coefficients and dipole moments for Ar–PF_3 and Kr–PF_3.

Transition	$\|M\|$	Ar–PF_3 $\Delta\nu/\mathscr{E}^2$ [a]	Ar–PF_3 o–c [b]	^{84}Kr–PF_3 $\Delta\nu/\mathscr{E}^2$	^{84}Kr–PF_3 o–c
0(0,0)–1(1,0)	0	2.723	−0.010		
1(0,1)–2(1,1)	0	3.900	−0.002	0.628	−0.018
	1	5.390	0.008	4.480	−0.033
2(0,2)–3(1,2)	0	−0.512	−0.002	2.100	−0.016
	1	−0.230	−0.003	2.480	0.003
	2	0.611	−0.007	3.610	0.052
3(0,3)–4(1,3)	0	3.195	−0.013		
	1	2.989	0.008		
	2	2.305	0.005		
	3	1.166	0.013		
5(0,5)–6(0,6)	0	−0.218	0.001		
	1	−0.189	−0.001		
	$\|\mu_a\|$	0.418(2) [c] D		0.491(7) D	
	$\|\mu_c\|$	0.942(1) D		0.933(8) D	
	$\|\mu_T\|$	1.031(2) D		1.055(14) D	

[a]Observed Stark coefficients in units of 10^5 MHz $(V/cm)^{-2}$.
[b]Observed–calculated Stark coefficients. The latter obtained with the dipole components below.
[c]The uncertainties are 2σ.

tives $(\partial I_{\alpha\beta}/\partial r_i)_e$ of the inertial tensor elements with respect to the internal coordinates.

In order to make the calculation tractable, we assumed that the internal force constants[11] of the PF_3 were unchanged upon complexation. Also, the interaction force constants between the PF_3 modes and the van der Waals modes were neglected. The internal coordinates r, θ, and ϕ describing the van der Waals modes are illustrated in Fig. 2. For C_s symmetry, there are 2 A' and 1 A'' van der Waals normal modes described by four quadratic force constants. Hence, four parameters could be determined $(f_{RR}^{-1}, f_{R\theta}^{-1}, f_{\theta\theta}^{-1}, f_{\phi\phi}^{-1})$ from the five τ's given in Table I. Finally, the effective structures of the complexes[1,2] and PF_3 [12] were used.

The calculation involves determining the **B** and **U** matrices which transform the Cartesian displacement coordinates to internal symmetry coordinates. The $\mathbf{G}^{-1}$ matrix (and **G**) and the derivatives $J_{\alpha\beta}$ were then obtained using matrix methods.

After the J's were calculated, Eq. (1) was used to fit the four van der Waals inverse force constants to the five τ's. The five different permutations of the fitting equations were used; the average of the five fits gave the force constants and their inverses listed in Table III.

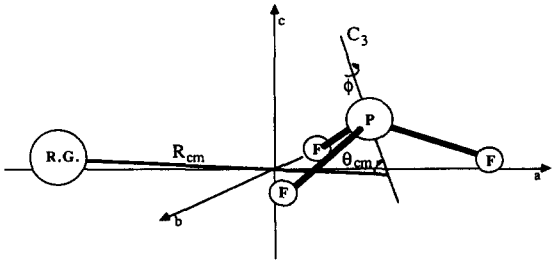

FIG. 2. Definition of internal coordinates $R_{c.m.}$, θ and ϕ used in the vibrational–centrifugal distortion analysis.

Calculations were repeated neglecting the force constants of PF_3. They show that $f_{RR}, f_{R\theta}, f_{\theta\theta}, f_{\phi\phi}$ decrease by approximately 0.3%, 7%, 4%, and 3%, respectively. Thus the PF_3 internal motions have a minor effect on the van der Waals force constants. These changes appear to be reasonable upper limit uncertainties for the force constants and vibrational frequencies.

With the **F** and **G** matrices known, a normal coordinate analysis was carried out to determine the frequencies of the normal modes (given in Table III), the **L** matrix which transforms the normal coordinates to internal coordinates and the $\mathscr{L}$ matrix which transforms the normal coordinates to mass-weighted Cartesian coordinates. The **L** matrix was used to calculate the root mean-square amplitudes of vibration at 0 K ($\Delta R_{rms} = \langle \Delta R^2 \rangle^{1/2}$) given in Table III. The $\mathscr{L}$ matrix was used to calculate the Coriolis coupling constants necessary to estimate the harmonic contributions to the vibration–rotation interaction of the molecule and the average moments of inertia. The average moments of inertia (I_{ii}^*) and the average structural parameters derived from them are reported in Table III. The largest uncertainties in the parameters arise from the approximations in the force field model and are estimated to be ± 0.005 Å in $R_{c.m.}$ and $\pm 0.2°$ in θ.

The changes between the effective and average structural parameters are small. It is noted that $(R_{c.m.})_{ave}$ is about 0.005 Å larger than $(R_{c.m.})_{eff}$ while $(\theta_{c.m.})_{ave}$ is about 1° smaller than $(\theta_{c.m.})_{eff}$ for all the species. The small difference in the angle between the Ar and Kr complexes (2°) appears real although it is difficult to identify its origin in any conclusive manner without examining the electronic interactions in some detail.

The stretching force constant f_{RR} can be used to approx-

TABLE III. Vibrational force constants, frequencies and mean square amplitudes of vibration for the van der Waals normal modes of Ar–PF_3 and Kr-PF_3; average moments of inertia (I_{ii}^*) and average structural (R^*, θ^*) parameters.

	Ar–PF_3	^{84}Kr–PF_3	^{86}Kr–PF_3
f_{RR}^{-1} (mdyn Å^{-1})$^{-1}$	60.67	51.86	51.96
$f_{R\theta}^{-1}$(mdyn)$^{-1}$	−1.45	−2.87	−3.19
$f_{\theta\theta}^{-1}$ (mdyn Å)$^{-1}$	91.78	65.22	67.58
$f_{\phi\phi}^{-1}$ (mdyn Å)$^{-1}$	61.92	55.65	55.56
f_{RR} (mdyn Å^{-1})	0.016 49	0.019 33	0.019 30
$f_{R\theta}$ (mdyn)	0.000 26	0.000 85	0.000 91
$f_{\theta\theta}$ (mdyn Å)	0.010 90	0.015 37	0.014 84
$f_{\phi\phi}$ (mdyn Å)	0.016 15	0.017 97	0.018 00
ω_R (cm^{-1})	31.8	27.6	27.4
ω_θ (cm^{-1})	18.1	20.9	20.5
ω_ϕ (cm^{-1})	19.6	20.3	20.3
ΔR_{rms} (Å)	0.153	0.136	0.135
$\Delta\theta_{rms}$ (deg)	10.21	9.70	9.74
$\Delta\phi_{rms}$ (deg)	7.14	6.83	6.83
I_{aa}^* (amu Å^2)	69.250 3	70.337 3	70.336 0
I_{bb}^* (amu Å^2)	495.429 7	778.629 5	787.152 8
I_{cc}^* (amu Å^2)	531.346 2	813.392 1	821.927 1
R_{cm}^* (Å)	3.959 5	4.077 4	4.077 1
θ_{cm}^* (deg)	69.303	67.253	67.269

imately estimate the binding energies of the complexes. By assuming a Lennard-Jones 6/12 potential to describe the angle-averaged radial interaction, it can be shown[13] that the well depth ϵ is given by $f_{RR}R_e^2/72$. By approximating R_e with $R^*_{\text{c.m.}}$, binding energies of 180 cm^{-1} and 224 cm^{-1} are obtained for the Ar and Kr species. The order of the stabilities is consistent with the relative polarizabilities of Kr and Ar. Nevertheless some caution is warranted since the binding energies estimated this way depend on the model assumed.

It is interesting to calculate the pure electrostatic contribution to the binding energy from a simple induced dipole-permanent field model as $\mu_{\text{ind}}^2/2\alpha$, where μ_{ind} is the induced moment of the rare-gas atom. For the Ar and Kr complexes, this gives 16.6 and 17.7 cm^{-1}, respectively. This suggests that the electrostatic interaction is not the dominant contributor to the binding energy.

Internal rotation barrier

An extensive search of the 7.5–13 GHz region was made for Ar–PF_3 mixtures, both to confirm the absence of internal rotation or tunneling splittings in the spectrum of Ar–PF_3 and to try to identify the spectra of species such as Ar_2–PF_3 and $(PF_3)_2$. The only extra transitions found have recently been assigned as PF_3–H_2O.[14] The $1_{10} \leftarrow 0_{00}$ transitions of both Ar–PF_3 and Kr–PF_3 showed some unresolved structure (~20–30 kHz) comparable to that observed for the $1 \leftarrow 0$ transition of PF_3 which we attribute to unresolved ^{31}P and ^{19}F spin–spin and spin rotation splitting. Given the nature of spectral searching in a narrow banded FTMW spectrometer one cannot be completely certain that tunneling splittings have not been missed or perhaps lie outside the search region. Nevertheless, we are more inclined to the view that any tunneling barriers are appreciable enough to dampen effects below the instrumental resolution.

An estimate of the V_3 barrier to internal rotation about the PF_3 symmetry axis below which discernable spectral effects might be expected can be obtained from solution of a one-dimensional Schrödinger equation for the Hamiltonian $-F\delta^2/\delta\phi^2 + V_3(1-\cos 3\phi)/2$. This indicates that a barrier of 50 cm^{-1} will lead to splittings of 10 kHz between the lowest states. An indication that the barrier is indeed above this is obtained from ω_ϕ in Table V and a harmonic approximation to the cos 3ϕ potential function.[15] This gives a barrier of 180 cm^{-1}. It is interesting, but perhaps fortuitous, that the difference in energy between structures C and D (Fig. 1) was calculated earlier by us[1] to be 97 cm^{-1} with C lower. This was a fixed geometry *ab initio* (6-21G, MP2) calculation and neither state was bound at this level.

Dipole moment

Two simple models have been used to rationalize the dipole moments of rare-gas complexes. In the case typified by Ar–OCS,[16] large amplitude vibrational averaging of the OCS dipole was invoked to explain the smaller moment of the complex compared to OCS. This is not applicable to the PF_3 systems; the small increase in the dipole moments for the PF_3 complexes (0.003 and 0.025 D, Ar, and Kr, respectively) and the rotation of the dipole moment away from the PF_3 symmetry axis (5.8° and 7.1°) cannot be reconciled with a harmonic vibrational averaging model.

A second approach is to estimate the induced moments in the rare gas using a polarization model and to add these to the components arising from the polar moiety. This worked reasonably well for Ar–N_2O using the known dipole and quadrupole moments of N_2O.[17]

In order to explore the polarization model, the observed dipole moment components of the complexes were decom-

TABLE IV. Experimental and calculated induced dipole moments (in D) of the rare-gas atom due to the electric field of PF_3 for conformations A–D in Fig. 1.

	Ar–PF_3			Kr–PF_3		
	$\mu_\perp$[a]	$\mu_\parallel$	$\lvert\mu_{\text{tot}}\rvert$	$\mu_\perp$	$\mu_\parallel$	$\lvert\mu_{\text{tot}}\rvert$
			Experimental[b]			
	0.104	−0.003	0.104	0.130	0.017	0.132
			Multipole[c]			
Dipole term	±0.026	−0.018	0.032	±0.039	−0.022	0.045
Quadrup. term	0.099	±0.199	0.222	−0.095	±0.280	0.296
A, B	−0.125	0.181	0.220	−0.134	0.258	0.291
C, D	−0.073	−0.217	0.229	−0.056	−0.302	0.307
			Ab initio[d]			
A	0.023	−0.032	0.039	0.037	−0.037	0.052
B	0.084	0.016	0.085	0.109	0.026	0.112
C	0.083	−0.016	0.085	0.114	−0.014	0.115
D	0.020	−0.067	0.070	0.041	−0.081	0.091

[a] $\mu_\parallel$ and $\mu_\perp$ (in D) are relative to the symmetry axis of PF_3.
[b] Determined from μ (RG) = μ (RG-PF_3) − μ (PF_3).
[c] Multipole expansion calculation; the contributions from the dipole and quadrupole moments of PF_3 are listed in the next two lines.
[d] Electric field at the rare gas site arising from the PF_3 calculated using GAUSSIAN86 (HF/6-31G*) WITH THE EXPERIMENTAL GEOMETRY OF PF_3 (REF. 12).

TABLE V. Measured ^{83}Kr nuclear coupling constants (χ_{aa}) and calculated electric field gradients (q_a^0) at the ^{83}Kr nuclear site for van der Waals complexes.

		$-eq_a^0/h$ (MHz/b)	
Complex	χ_{aa} (MHz)	I[a]	II[b]
^{83}Kr–OCS	1.601(7)[c]	—	0.2282
^{83}Kr–HCl	5.20(10)[d]	0.2629(402)[d]	0.2813
^{83}Kr–HCN	7.46(5)[d]	0.3971(1013)[d]	0.4053
^{83}Kr–HF	10.23(8)[d]	0.4987(575)[d]	0.4937
^{83}Kr–ClF	13.90(25)[e]	0.5110[e]	0.6624
^{83}Kr–PF_3	4.31		
A[f]			−0.0112
B			−0.3267
C			0.3221
D			−0.0153

[a] q_a^0 is calculated from an explicit multipole expansion.
[b] q_a^0 is from an *ab initio* calculation of the partner molecule at the HF/6-31G** level for HCl, HCN and HF and the HF/6-31G* level for OCS, ClF and PF_3. Structures taken from the references cited in the table.
[c] F. J. Lovas and R. D. Suenram, J. Chem. Phys. **87**, 2010 (1987).
[d] Reference 26.
[e] Reference 28.
[f] Structures A–D for Kr–PF_3, see Fig. 1.

posed into that contributed by the PF_3 (no correction for vibrational averaging) and that due to an induced polarization of the rare gas. The rare gas components are labeled as the experimental $\mu_\perp$ and $\mu_\parallel$ in Table IV; parallel and perpendicular are defined relative to the symmetry axis of PF_3. The signs are consistent with the negative direction in PF_3 towards the fluorine end (likewise throughout this discussion). The values for the induced dipole moment μ_{ind} in the four conformations were then calculated using the program Mathematica[18] from the equations

$$\mu_{ind} = \alpha \mathbf{E},$$

$$\mathbf{E} = -\nabla\left[\frac{\mu\cdot\mathbf{R}}{|\mathbf{R}|^3} + \frac{\mathbf{R}\cdot\Theta\cdot\mathbf{R}}{|\mathbf{R}|^5}\right],$$

where α is the polarizability of Ar (1.6411 Å^3)[19] or Kr (2.4844 Å^3),[19] μ and Θ are the permanent dipole (1.029 D)[20] and quadrupole moments ($\Theta_{zz} = 24.1 \times 10^{-26}$ esu cm^2 = 24.1 D Å)[21] of PF_3, and R is the $R_{c.m.}$ vector for the four conformations consistent with the structural parameters in Table III. The results are listed in Table IV under multipole, where μ_{ind} is decomposed into $\mu_\parallel$ and $\mu_\perp$ for the dipole and quadrupole terms. It is seen that the calculated values are substantially different from the observed values in both magnitude and direction for all four structures A–D. There are several possible reasons for this discrepancy. The neglect of the higher moments of PF_3 and/or the assumption that the center of mass of PF_3 is also the center of the dipolar and quadrupolar fields seem the most likely factors. The neglect of the induced polarization of the PF_3 and vibrational averaging effects contribute somewhat although rough estimates indicate that this is less than 0.05 D. The breakdown of the "far-field" approximation may also be a factor.

An alternative approach is to estimate the electric field at the rare gas site using *ab initio* methods in an effort to compensate for some of the deficiencies noted above. We used the GAUSSIAN86[22] program and a 6-31G* basis set to calculate at the self consistent field (HF) level the electric field arising from PF_3 at the position of the rare gas for conformations A–D for both the Ar and Kr complexes. The rare gas polarizabilities mentioned above were used with the calculated fields to obtain the induced dipole moments labeled *ab initio* in Table IV. In this case the relative values of $\mu_\perp$ and $\mu_\parallel$ as well as their magnitudes are in much better agreement with experiment for conformations B and C. Since B is an unlikely conformation for other reasons (the Ar–F distance is approximately 0.75 Å shorter than the sum of their van der Waals radii), this approach reduces the possibilities to a single preferred conformation. Nevertheless, the reliability of this argument might be questioned since it is not clear how accurately the electric fields can be estimated from this level of wave function. Given that the calculated dipole moment of PF_3 at the HF/6-31G* level using the experimental geometry is 1.32 D, which is too large by about 28%, it would appear that the calculated fields are reliable enough to trust the distinctions made in Table IV between conformations B,C vs A,D. Another uncertainty arises from the treatment of the argon as a point polarizable atom, i.e., from the neglect of the variation of the electric field over the volume of the argon atom. This point was not explored since another approach to resolving the structural question was available. This approach will be discussed next.

^{83}Kr nuclear quadrupole coupling analysis

The ^{83}Kr nuclear quadrupole coupling constants (Table I) provide another probe of the electronic structure of the Kr–PF_3 complex. A comparison of the experimental values with predicted values for structures A–D offers another possibility to identify the correct conformation. The quadrupole coupling constant along a principal inertial axis is given by

$$\chi_{ii} = -eQ^{Kr}q_i/h, \tag{2}$$

where e and h have their usual meaning, Q^{Kr} is the nuclear quadrupole moment of ^{83}Kr and q_i is the component of the electric field gradient tensor along the inertial axis ($i = a,b,c$). Since the value of Q^{Kr} is known to approximately 15% accuracy, the task of predicting the values of χ_{ii} reduces to estimating values of q_i for the various conformations.

In a free rare-gas atom, the electronic charge distribution is spherically symmetric, that is, the electric field gradient at the nucleus is zero. Thus, the finite values of χ arise from the van der Waals interaction. Following the analysis of Sternheimer *et al.*,[23–25] the contributions to q_i come from the distortion of the closed shells of ^{83}Kr by the partner molecule and charge distributions lying outside ^{83}Kr. Assuming that there is no charge transfer or orbital overlap, the electric field gradient at the rare-gas nuclear site is given by

$$q_i = q_i^0(1 - \gamma_\infty), \tag{3}$$

where q_i^0 is the contribution from the charges external to Kr. The external charges produce a proportional contribution from distortion of the Kr filled shell given by $q_i^0\gamma_\infty$ where γ_∞ is the Sternheimer shielding factor, which is specific to each atom or ion.

In previous studies of ^{83}Kr, ^{131}Xe and ^{201}Hg van der Waals complexes,[26–30] the electric field gradient q_i^0 was estimated from the electric multipole moments of the partner molecule in an explicit multipole expansion. Since only the dipole and quadrupole moments of PF_3 are known, this procedure will not distinguish between structures A and B or between C and D. Higher moments are needed to incorporate the electric field asymmetries implicit in the four distinct conformations. An alternative approach is to use an *ab initio* calculation for the partner molecule to estimate the field gradient it produces at the coordinates of the rare gas in the complex.

Before examining Ar–PF_3, we explored this procedure for several complexes in the literature. We list in Table V the measured nuclear coupling constants along the inertial a axis and the electric field gradients at the ^{83}Kr nucleus calculated by the explicit multipole expansion[26,28] and the *ab initio* approach at the HF/6-31G** level, using the GAUSSIAN86 program. The electric field gradient is calculated along the line (axis) joining the rare-gas to the center-of-mass of the partner instead of the a axis. The two axes are only slightly different from each other for all the complexes, resulting in a negligible error for our purposes in the calculated q_i^0. Com-

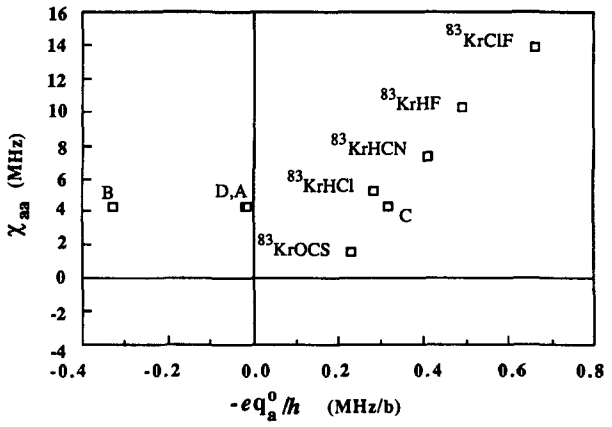

FIG. 3. The observed quadrupole coupling constants χ_{aa} for ^{83}Kr complexes plotted vs $-eq_a^0/h$ where the field gradient q_a^0 at the Kr site was obtained from an *ab initio* calculation of the partner molecule ($b = 1\times10^{-24}$ cm^2).

paring the calculated electric field gradients from the two methods (Table V), we see that they are in reasonable agreement for ^{83}Kr–HCl, HCN, HF; but not for ^{83}Kr–ClF. This may be due to neglect of higher moments in the multipole expansion calculation of q_i^0. The *ab initio* value was more sensitive to the level of calculation for ^{83}Kr–ClF than the others and may also not be an optimal estimate. The electric field gradient arising from the PF_3 at the four possible sites for the ^{83}Kr nucleus in the complex (Fig. 1) were calculated at the HF/6-31G* level and are reported in Table V.

In Fig. 3, the measured ^{83}Kr nuclear quadrupole coupling constant χ_{aa} is plotted as a function of the *ab initio* field gradient $-eq_i^0/h$ for the complexes in Table V and the four structures of ^{83}Kr–PF_3. If Eq. (2) is strictly obeyed, the points should lie on a straight line which intersects the origin. It is seen that the points for the ^{83}KrHCl, HCN, HF, ClF, and OCS complexes along with structure C approximately obey this relationship. The scatter presumably arises from errors in the calculated q_i^0 for several of the complexes. One possibility is that the calculated values for ^{83}KrHCl, HCN, HF, and ClF which approximately extrapolate to the origin of the coordinate system are close to correct while those for ^{83}KrOCS and structure C are less reliable. Another possibility is that a linear relationship is observed which does not go through the origin signifying some charge transfer contributions to χ_{aa}. We prefer the first possibility (see below), but in either case, the marked displacement of the points for structures A, B and D from the rest of the values indicates that only structure C satisfies the Sternheimer model. Calculations of q_i^0 for ^{83}Kr–PF_3 were also made using 6-311G* and STO-3G basis sets. Structures A, C and D were not very sensitive to the basis set while for structure B, $-eq_i^0/h$ was even more negative. Hence, the conclusion that the calculated q_i^0 are compatible with χ_{aa} only for structure C is unlikely to change as the calculated value improves.

For structure C, we examined the variation of the calculated electric field gradients at the Kr site along the *a*, *b* and *c* inertial axes arising from PF_3 and the PF_3 dipole moment for the three basis sets cited above. The values shown in Table VI indicate a quasi-linearity of μ vs $-eq_i^0/h$ signifying a correlation between the electric field gradient and the dipole moment. This led to an estimate of the electric field gradients from the observed dipole moment by a linear extrapolation and the results are listed in Table VI as the scaled values. The uncertainties are determined by the different levels of calculation and the observed dipole moment. These values of $-eq_i^0/h$ are plotted vs the observed χ_{ii} in Fig. 4. The three data points are aligned and yield a slope of 16.4(2) b (1 b $= 10^{-24}$ cm^2) and intercept of 0.057(37) MHz, where the numbers in parentheses represent one standard deviation. The intercept can be used to estimate an upper limit for charge transfer in Kr–PF_3, using a Townes and Dailey type argument.[31] Using a conversion of 750 MHz per electron for the 4*p* orbital from Buxton *et al.*,[27] this corresponds to a fractional electron transfer of $\sim 1\times10^{-4}$ or less. We conclude that there is very little charge transfer, if any, in the complex.

The direct proportionality observed here between q_i and q_i^0 for the ^{83}Kr–PF_3 system can be understood qualitatively as arising from Sternheimer type quadrupolar shielding occurring in the ^{83}Kr atom. Although it is not possible to convert our slope automatically to γ_∞ for ^{83}Kr,[26] it is still interesting to convert it into an effective shielding factor. Using Eqs. (2) and (3) and the nuclear quadrupole moment of 0.27 b[32,33] for the ^{83}Kr nucleus, a value of $-59.7(7)$ is obtained for the ^{83}Kr shielding parameter. The quoted error does not include the uncertainty in Q^{Kr} of roughly 15%. A previous estimate of the shielding parameter for Kr complexes using a similar procedure gave $-77.5(150)$.[26] A nonrelativistic frozen-core calculation[34] gave $\gamma_\infty = -67$ with an error of 15% and a calculation[35] based on relativistic Hartree–Fock–Slater electron theory gave $\gamma_\infty = -84$ with an error of 7%.

TABLE VI. Calculated dipole moments of PF_3 and electric field gradients along the *a*, *b*, and *c* axes for structure C (Fig. 1) of ^{83}Kr–PF_3.

	μ (D)	$-eq_a^0/h$ (MHz/b)	$-eq_b^0/h$ (MHz/b)	$-eq_c^0/h$ (MHz/b)
HF/6-311G*	1.6174	0.3740	−0.2063	−0.1677
HF/6-31G*	1.3119	0.3221	−0.1751	−0.1470
HF/STO-3G	1.2378	0.3035	−0.1713	−0.1322
Scaled	1.029(10)[a]	0.2632(107)	−0.1530(66)	−0.1102(171)

[a] Observed dipole moment value for PF_3.

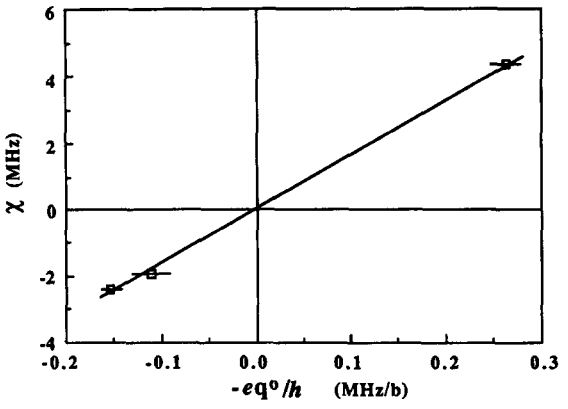

FIG. 4. The observed values of χ_{ii} for Kr–PF_3 plotted vs the values of $-eq_i^0/h$ obtained from scaling the calculated values of q_i^0 using the dipole of PF_3.

IV. SUMMARY

Our analyses of the dipole moment for the Ar and Kr complexes with PF_3 and the quadrupole coupling constants for ^{83}Kr–PF_3 have compared the experimental results with values extrapolated from *ab initio* calculations of the electric field and its gradient for PF_3. The comparisons along with the similarities in $R_{c.m.}$ and $\theta_{c.m.}$ argue persuasively that structure C corresponds to the observed species for both the Ar and Kr complexes. The van der Waals interaction appears to be explained well by an electrostatic model with very little charge transfer. The use of *ab initio* calculations for the partner molecule as a means of interpreting the induced dipole moments and quadrupole coupling constants of the rare-gas atom has been used here for the first time and proves to be a very useful supplement to the experimental results, especially to resolve the conformational ambiguities which arise from the inertial analysis. A supermolecule calculation can in principle also resolve the conformational ambiguity. Such a calculation has been done for Ar–PH_3 and finds structure C also the most stable[36(a)]; however, the Ar–PF_3 system has proven to be a more difficult calculation and convergence difficulties prohibit a firm conclusion at this time.[36(b)] Our earlier *ab initio* calculation (confer above: internal rotation section) indicated that A was the lowest energy conformation; this inconsistency with the present analysis presumably arises from the level of calculation (6-21G, MP2) and neglect of basis set superposition errors.

ACKNOWLEDGMENT

This work was supported by Grants Nos. CHE-8305806 and CHE-8614340 from the National Science Foundation.

[1]K. W. Hillig II, J. Matos, A. Scioly, and R. L. Kuczkowski, Chem. Phys. Lett. **133**, 359 (1987).
[2]M. S. Labarge, E. R. Bittner, K. W. Hillig II, and R. L. Kuczkowski, J. Mol. Struct. **189**, 105 (1988).
[3]R. K. Bohn, K. W. Hillig II, and R. L. Kuczkowski, J. Phys. Chem. (in press).
[4]J. S. Muenter, J. Chem. Phys. **48**, 4544 (1968).
[5]W. Gordy and R. L. Cook, *Molecular Microwave Spectra* (Wiley, New York, 1984), Chap. 8.
[6]V. Typke, J. Mol. Spectrosc. **63**, 170 (1976).
[7]Ref. 5, pp. 413–418.
[8]S. N. Ghosh, R. Trambarulo, and W. Gordy, J. Chem. Phys. **21**, 308 (1953).
[9]D. R. Herschbach and V. W. Laurie, J. Chem. Phys. **37**, 1668,1687 (1962).
[10](a) J. A. Shea, W. G. Read, and E. J. Campbell, J. Chem. Phys. **79**, 2559 (1983); (b) M R. Keenan, D. B. Wozniak, and W. H. Flygare, *ibid.* **75**, 631 (1981).
[11]C. E. Small and J. G. Smith, J. Mol. Spectrosc. **73**, 215 (1978).
[12]Y. Kawashima and A. P. Cox, J. Mol. Spectrosc. **65**, 319 (1977).
[13]P. D. Aldrich, A. C. Legon, and W. H. Flygare, J. Chem. Phys. **75**, 2126 (1981).
[14]M. S. LaBarge, K. W. Hillig II, and R. L. Kuczkowski (unpublished results).
[15]Ref. 5, pp. 570–581.
[16]S. J. Harris, K. C. Janda, S. E. Novick, and W. Klemperer, J. Chem. Phys. **63**, 881 (1975).
[17]C. H. Joyner, T. A. Dixon, F. A. Baiocchi, and W. Klemperer, J. Chem. Phys. **75**, 5285 (1981).
[18]S. Wolfram, *Mathematica: A System for Doing Mathematics* (Addison-Wesley, New York, 1988); Wolfram Research Inc., Champaign, Illinois.
[19]R. H. Orcutt and R. H. Cole, J. Chem. Phys. **46**, 697 (1967).
[20]This work.
[21]R. G. Stone, J. M. Pochan, and W. H. Flygare, Inorg. Chem. **8**, 2647 (1969).
[22]M. J. Frisch, J. S. Binkley, H. B. Schlegel, K. Raghavachari, C. F. Melius, R. L. Martin, J. J. P. Stewart, F. W. Bobrowicz, C. M. Rohlfing, L. R. Kahn, D. J. DeFrees, R. Seeger, R. A. Whiteside, D. J. Fox, E. M. Fluder, and J. A. Pople, GAUSSIAN86 (Carnegie-Mellon Quantum Chemistry Publishing Unit, Pittsburgh, PA, 1986).
[23]R. M. Sternheimer, Phys. Rev. **80**, 102 (1950); **84**, 244 (1951); **86**, 316 (1952); **95**, 736 (1954).
[24]R. M. Sternheimer and H. M. Foley, Phys. Rev. **92**, 1460 (1953); **102**, 731 (1956).
[25]H. M. Foley, R. M. Sternheimer, and D. Tycko, Phys. Rev. **93**, 734 (1954).
[26]E. J. Campbell, L. W. Buxton, M. R. Keenan, and W. H. Flygare, Phys. Rev. A **24**, 812 (1981).
[27]L. W. Buxton, E. J. Campbell, M. R. Keenan, T. J. Balle, and W. H. Flygare, Chem. Phys. **54**, 173 (1981).
[28]L. W. Buxton, E. J. Campbell, and W. H. Flygare, Chem. Phys. **59**, 55 (1981).
[29]E. J. Campbell, L. W. Buxton, and A. C. Legon, J. Chem. Phys. **78**, 3483 (1983).
[30]J. A. Shea and E. J. Campbell, J. Chem. Phys. **81**, 5326 (1984).
[31]C. H. Townes and B. P. Dailey, J. Chem. Phys. **17**, 782 (1949).
[32]W. L. Faust and L. Y. Chow Chiu, Phys. Rev. **129**, 1214 (1963).
[33]X. Husson, J.-P. Grandin, and H. Kucal, J. Phys. B **12**, 3883 (1979).
[34]R. P. McEachran, A. D. Stauffer, and S. Greita, J. Phys. B **12**, 3119 (1979).
[35]F. D. Feiock and W. R. Johnson, Phys. Rev. **187**, 39 (1969).
[36](a) Z. Latajka and S. Scheiner, J. Mol. Struct. (in press); (b) private communication.
[37]See AIP document no. PAPS JCPSA-90-6949-5 for 5 pages of tables of Ar–PF_3 and ^{83}Kr–PF_3. Order by PAPS number and journal reference from American Institute of Physics, Physics Auxiliary Publication Service, 335 East 45th Street, New York, NY 10017. The price is $1.50 for each microfiche (98 pages) or $5.00 for photocopies of up to 30 pages, and $0.15 for each additional page over 30 pages. Airmail additional. Make checks payable to the American Institute of Physics.